ACS APPLIED MATERIALS & INTERFACES

Research Article

www.acsami.org

Ion-Exchange Polymer Nanofibers for Enhanced Osteogenic Differentiation of Stem Cells and Ectopic Bone Formation

Iman Shabani,[†] Vahid Haddadi-Asl,*[,†] Masoud Soleimani,[‡] Ehsan Seyedjafari,[⊥] and Seyed Mahmoud Hashemi[§]

[†]Department of Polymer Engineering and Color Technology, Amirkabir University of Technology, Tehran, Iran

[‡]Department of Hematology, Faculty of Medical Sciences, Tarbiat Modares University, Tehran, Iran

[§]Department of Stem Cell Biology, Stem Cell Technology Research Center, Tehran, Iran

[⊥]Department of Biotechnology, College of Science, University of Tehran, Tehran, Iran

ABSTRACT: Nanofibrous scaffolds with specific modifications have shown promising potential for bone tissue engineering applications. In the present study, poly(ether sulfone) (PES) and sulfonated PES (SPES) nanofibers were fabricated via electrospinning. Calcium ions were then incorporated in SPES by immersion in a $Ca(OH)_2$ solution. The calcium-ion-exchanged SPES (Ca-SPES), PES, and SPES nanofibers were characterized and then evaluated for their osteogenic capacity: both in vitro using stem cell culture and in vivo after subcutaneous implantation in mice. After 7 days of immersion in simulated body fluid, the formation of an apatite layer was only observed on Ca-SPES nanofibers. According to the MTT results, an increasing stem cell population was detected on all scaffolds during the period of study. Using real-time reverse transcriptase−polymerase chain reaction, alkaline phosphatase activity, and calcium content assays, it was demonstrated that the osteogenic differentiation of stem cells was higher on Ca-SPES scaffolds in comparison with PES and SPES nanofibers. Interestingly, Ca-SPES scaffolds were shown to induce ectopic bone formation after 12 weeks of subcutaneous implantation in mice. This was confirmed by mineralization and the production of collagen fibers using van Kossa and Masson's trichrome staining, respectively. Taken together, it was demonstrated that the incorporation of calcium ions into the ion-exchange nanofibrous scaffolds not only gives them the ability to enhance osteogenic differentiation of stem cells in vitro but also to induce ectopic bone formation in vivo.

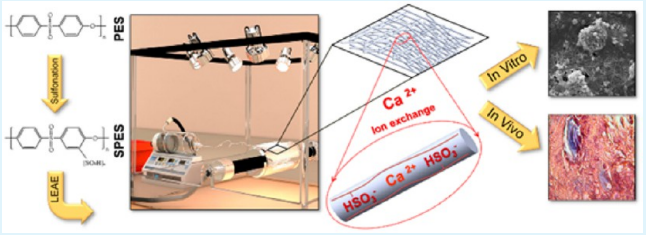

KEYWORDS: *nanofiber, ion-exchange polymer, electrospinning, stem cell, osteogenic differentiation, calcium ion*

INTRODUCTION

Recently, an increasing trend is arising for the utilization of bone graft substitutes (BGSs). It is due to both the requirement of more than two million grafting procedures for the repair of bone damages worldwide and the well-known challenges concerning the use of autografts and allografts. An ideal BGS is considered to have the following properties: (1) osteoconductivity, which is defined as the potential of BGSs to provide a matrix or scaffold for bone formation, (2) osteoinductivity, which is the ability of a material to induce bone formation in nonosseous tissues, (3) osteogenic cells such as stem cells, progenitors, or mature osteoblasts, which produce the new bone matrix, and (4) osteointegration, which is defined as the ability of a material to bond chemically to the host tissue without formation of an intervening fibrous tissue.[1−3]

In order to fully support the neo-tissue formation, BGSs should also have structural integrity and appropriate mechanical properties during bone healing.[4] Many research groups have attempted to design and develop new synthetic BGSs that possess as many characteristics of an ideal BGS as possible. A variety of materials have been used to fabricate BGSs such as metals,[5] hydroxyapatite,[6] a demineralized bone matrix,[7] peptide amphiphiles,[8] and bioactive glasses.[9−11] Recently, our research group has proposed poly(ether sulfone) (PES) as a new substrate for the preparation of BGSs.[12] PES is a noncytotoxic polymer that has been used in biomedical applications such as hemodialysis membranes, ultrafiltration, and also hollow fibers in bioartificial bioreactors for tissues such as liver and kidney.[13,14]

Besides material selection, the fabrication technique is also important to create an efficient BGS with appropriate characteristics enhancing bone regeneration and repair. Among the different methods for synthetic graft preparation, electrospinning has attracted the interest of the research community. This method has valuable characteristics such as simplicity, cost-effectiveness, and also the ability to produce nanofibrous scaffolds mimicking the physical structure of the native extracellular matrix (ECM).[15,16] In the past decade, electrospun mats have been widely used as BGSs and as tissue-engineered scaffolds for the regeneration of defects in tissues,

Received: June 27, 2013
Accepted: December 16, 2013
Published: December 16, 2013

   dx.doi.org/10.1021/am404500c | ACS Appl. Mater. Interfaces 2014, 6, 72−82

such as bone,[1718]cartilage,[19,20] skin,[21,22] muscle,[23] etc. Despite their advantages, the two-dimensional nature of the electrospun scaffolds have always been indicated as a major drawback for their applications in the reconstruction of three-dimensional (3D) tissues. Therefore, there have been several attempts to address this issue.[24−27] In a most recent experiment, we developed a modified technique, termed light emission array electrospinning (LEAE), to create 3D electrospun membranes. The scaffolds fabricated by LEAE were demonstrated to support excellent infiltration and proliferation of stem cells throughout the nanofibers.[28]

Calcium phosphate-based materials are the most attractive BGSs probably because of their similar composition to native bone.[29] These materials provide the formation of an apatite layer on their surface through the release of calcium ions, resulting in a bridging between BGSs and the host bone, which helps osteointegration and tissue in-growth.[30] Calcium ions have also been reported to significantly influence osteoblast proliferation, matrix maturation, mineralization, and regulation.[31] Interestingly, in a recent report, it was demonstrated that the increased concentration of calcium ions in a culture medium enhanced biomineralization of mesenchymal stem cells derived from adipose tissue.[32] Elevated concentrations of calcium ions were shown to induce the upregulation of bone-specific genes such as BMP2 and osteocalcin.[33]

In our previous research, we suggested a PES electrospun membrane as an appropriate choice for BGS applications.[12] In the present study, we hypothesized that the incorporation of calcium ions into the ion-exchange nanofibers would produce a bioactive BGS that could be considered efficient for bone regeneration applications. To produce ion-exchange scaffolds, PES was functionalized with sulfonic acid groups and then electrospun into nanofibers. This method of modification was previously used to enhance the formation of an apatite layer on the surface of polymers, such as poly(ethylene terephthalate), Nylon 6, polyethylene, and polystyrene.[34,35] However, for the first time, we evaluated the ability of this novel BGS to support osteogenic differentiation of stem cells in vitro. In addition, osteoinduction and bone formation in subcutaneous tissue of mice models were investigated in vivo. Moreover, LEAE was used to fabricate nanofibrous membranes with 3D and cellular infiltration characteristics.

EXPERIMENTAL SECTION

Polymer Synthesis and Characterization. The sulfonation process of poly(ether sulfone) (PES; Ultrason E6020P, BASF, Ludwigshafen, Germany) was performed based on the procedure as previously reported.[36] Briefly, PES was initially dissolved in concentrated sulfuric acid (Merck, Germany) under vigorous stirring at 25 °C for 5 h. Subsequently, chlorosulfonic acid (Merck, Darmstadt, Germany) was added dropwise to the resultant solution under vigorous stirring at 5 °C, and the mixture was stirred for a determined reaction time. Then, the mixture was precipitated in deionized water, and the polymer was recovered by filtration and washed several times with deionized water until the pH was neutral. Finally, the samples were vacuum dried at 100 °C for 12 h.

Chemical modifications after sulfonation of PES were investigated by Fourier transform infrared spectroscopy (FTIR). The spectra were recorded using an Equinox 55 spectrometer (Bruker Optics, Ettlingen, Germany) equipped with a deuterated triglycine sulfate detector. The degree of sulfonation was measured quantitatively via acid−base titration, according to the procedure described by Kim et al.[37]

For proton conductivity measurements, PES and SPES samples were dissolved in *N*,*N*-dimethylformamide (DMF; Merck, Darmstadt, Germany) and cast onto glass plates. After incubation at 70 °C for 10 h, the final drying step was carried out at 120 °C for 12 h. The proton conductivity of fully hydrated membranes was measured at room temperature via alternating-current impedance using a Solartron Interface 1260 gain phase analyzer over the frequency range of 1−10^6 Hz. The proton conductivity was measured at constant relative humidity of 95% using 4-point probe method measurement.

Prior to electrospinning, a Brookfield DV-III programmable viscometer and a Metrohm 712 conductometer were used to measure the viscosity and conductivity of the solutions, respectively.

Scaffold Fabrication and Characterization. Synthesized sulfonated PES (SPES) samples with a definite degree of sulfonation were used for scaffold fabrication. According to our previous study, LEAE was performed to construct PES and SPES nanofibrous webs.[28] Electrospinning solutions were prepared by dissolving each polymer in a certain amount (25 wt %) in DMF. A 10 mL disposable syringe was used to stock each of the prepared solutions. A syringe pump was used to feed the solution through an extension tube ending in a blunted 21-gauge needle. To collect the nanofibers, a cylindrical stainless steel collector was located at 15 cm from the needle. A high voltage potential (20 kV) was also applied between the needle and collector. With initiation of the electrospinning process and the effect of the high voltage, the polymeric solution is forced to leave the tip of the needle and be collected as nanofibers on the rotatory cylinder. The nanofibrous membranes were then separated from the collector surface and used for further analysis and application.

To produce calcium-ion-exchanged SPES nanofibers (Ca-SPES), the fabricated SPES nanofibers, in proton form, were treated with a calcium hydroxide [$Ca(OH)_2$] solution. In order to conduct the exchange of protons with calcium ions, substrates were soaked in a saturated $Ca(OH)_2$ solution for 48 h at 25 °C and rinsed with distilled water until the pH level became neutral. To investigate the bioactivity, fabricated scaffolds were soaked in simulated body fluid (SBF) with ion concentrations approximately equal to those of human plasma for 7 days.[38]

To evaluate the porosity of the scaffolds, five randomized circular samples with diameter of 20 mm were used, and the estimated porosity of each sample was calculated by the following equation: porosity = 1 − (calculated membrane density/known material density) × 100.

To measure the specific surface area of the nanofibers, the Brunauer−Emmett−Teller (BET) method by a BELSORP (BEL Japan Inc., Osaka, Japan) apparatus was used. Nitrogen adsorption−desorption isotherms of nanofibers were obtained, and the specific surface area was calculated from the BET plot of the isotherms by *BELSORP* software.

Isolation, Culture, and Differentiation of Human Mesenchymal Stem Cells (MSCs). Human MSCs were isolated from the bone marrow aspirates of a donor after informed consent according to a procedure described previously.[39] The aspirate was diluted at 1:3 in a Dulbecco's modified Eagle's medium (DMEM; Gibco, Paisley, U.K.). Bone marrow suspensions were overlaid on a Ficoll-Hypaque density gradient (1.077 g mL^{-1}, Sigma-Aldrich Inc., St Louis, MO) and centrifuged at 500 g for 20 min. The mononuclear cell layer was removed from the interface, washed twice with phosphate-buffered saline (PBS; Gibco, Paisley, U.K.), and resuspended in DMEM at a density of 10^7 mL^{-1}. The cells were allowed to adhere overnight at 37 °C with 5% humidified CO_2 in culture flasks (Nunc, Roskilde, Denmark). Each flask contained DMEM supplemented with 20% fetal bovine serum (FBS; Gibco, Paisley, U.K.), 100 U mL^{-1} penicillin, 100 μg mL^{-1} streptomycin, and 2.5 μg mL^{-1} amphotericin B. On day 1, nonadherent cells were discarded and adherent cells were washed with PBS and cultured. At approximately 50% confluence, the cells were replated and used for further studies. For osteogenic differentiation, the cells were cultured in DMEM supplemented with 10% FBS, 10^{-8} M dexamethasone, 0.2 mM ascorbic acid 2-phosphate (Sigma), and 10 mM β-glycerophosphate (Sigma).

Cell Seeding. Prior to cell seeding, circular scaffolds were immersed overnight in 70% ethanol for sterilization and then in a culture medium to ensure sterilization and enhance cell attachment after seeding. In addition to tissue culture polystyrene (TCPS), a

dx.doi.org/10.1021/am404500c | ACS Appl. Mater. Interfaces 2014, 6, 72−82

commercial BGS named CenoBone (Tissue Regeneration Corp., Kish, Iran) was used as a control. An initial cell density of 5×10^4 cm^{-2} of scaffolds was suspended in 75 μL of the medium, seeded onto the top of the circular scaffolds, TCPS, and CenoBone, and incubated for 2 h. The cell culture was performed in 24-well plates, and in order to immerse the scaffolds completely, 500 μL of the medium was used and replaced every 2 days. The cells on these scaffolds were incubated under an osteogenic medium for 2 weeks.

Scanning Electron Microscopy (SEM). The scaffold surfaces were analyzed using a scanning electron microscope (VEGA II, TESCAN, Brno, Czech Republic) equipped with an energy-dispersive electron X-ray spectroscopy (EDX) instrument (INCA, Oxford Instruments, Abingdon, U.K.). The mapping mode was performed on the surface of the scaffolds to detect the existence of specific elements, such as calcium and phosphorus. Before SEM experiments, the specimens were coated with gold and palladium using a sputter coater. The fiber diameter was determined from SEM images using image analysis software. The morphology of MSC on the scaffolds during osteogenic differentiation was also investigated by SEM. The cell-loaded scaffolds were rinsed with PBS after 7 and 14 days of osteogenic differentiation and fixed in 2.5% glutaraldehyde for 1 h. The samples were dehydrated in graded series of alcohol and then dried.

3-(4,5-Dimethylthiazol-2-yl)-2,5-diphenyltetrazolium Bromide (MTT) Assay. Proliferation of MSC on different scaffolds and CenoBone was evaluated via MTT assay. Sterilized nanofibrous membranes were placed in a 24-well culture plate, seeded with a cell density of 5×10^3 cells cm^{-2}, and incubated at 37 °C, 5% CO_2. After 1, 2, 3, 4, and 5 days of cell seeding, 50 μL of the MTT solution (5 mg mL^{-1} in DMEM) was added to each well (n = 5). For conversion of MTT to formazan crystals by mitochondrial dehydrogenases of living cells, the plate was incubated at 37 °C for 3 h. For dissolution of the dark-blue intracellular formazan crystals, the supernatant was removed and a constant amount of an appropriate solvent was added. The optical density (OD) was read spectrophotometrically at a wavelength of 570 nm. The same procedure was performed for cultured MSC on TCPS as the control.

To investigate the infiltration of stem cells, cell-loaded scaffolds were cross-sectioned, stained with hematoxylin and eosin (H&E), and observed under a light microscope.

Real-Time Reverse Transcriptase–Polymerase Chain Reaction (RT-PCR). To quantify the difference between the mRNA levels of osteogenic markers, gene expression in MSC on scaffolds and TCPS was analyzed using real-time RT-PCR. Total RNA was purified using an RNeasy kit (Qiagen, Germantown, MD), according to the manufacturer's specifications and including the optional DNase treatment. cDNA synthesis was carried out using Revert Aid first strand cDNA synthesis kit (Fermentas, Burlington, Ontario, Canada). Then the synthesized cDNA was used for 40-cycle PCR in a Rotor-gene Q real-time analyzer (Corbett, Germantown, MD). Real-time RT-PCR was performed using SYBR Premix Ex Taq (Takara, Japan) followed by melting-curve analysis to confirm the PCR specificity. Each reaction was repeated three times, and the threshold cycle average was used for data analysis by *Rotor-gene Q* software (Corbett, Germantown, MD). Genes and related specific primers are illustrated in Table 1. The relative expression was quantified using the ΔΔCt method. Target genes were normalized against β-actin and calibrated to MSC (passage 2).

Table 1. Primers for Real-Time RT-PCR

gene	primer sequence (F,R, 5′→ 3′)	product length (bp)
β-actin	CTTCCTTCCTGGGCATG	85
	GTCTTTGCGGATGTCCAC	
osteocalcin	GCAAAGGTGCAGCCTTTGTG	80
	GGCTCCCAGCCATTGATACAG	
runx2	GCCTTCAAGGTGGTAGCCC	67
	CGTTACCCGCCATGACAGTA	

Alkaline Phosphatase (ALP) Activity and Calcium Content Assay. In order to assay the activity of ALP, the total protein of cells cultured on the TCPS, CenoBone, and scaffolds was extracted using 200 μL of a RIPA lysis buffer. For sedimentation of cell debris, the lysate was centrifuged at 14000g at 4 °C for 15 min. After that, supernatant was collected and the ALP activity was measured using p-nitrophenyl phosphate as the substrate. The enzyme activity level (IU) was normalized against the total protein.

The amount of calcium deposited on TCPS, CenoBone, and different scaffolds during osteogenic differentiation was measured using the cresolphthalein complex one method. Calcium extraction was performed by homogenization of the scaffolds in 0.6 N hydrochloric acid (Merck) followed by shaking for 4 h at 4 °C. The OD was obtained at 570 nm after addition of the reagent to calcium solutions. The calcium content was measured from the standard curve of the OD versus a serial dilution of calcium concentrations. To visualize calcium accumulations, TCPS and scaffolds were stained with Alizarin Red S and investigated under a light microscope.

Subcutaneous Implantation. All animal experiments were performed in accordance with the Stem Cell Technology Research Center (Tehran, Iran) guidelines. Male Balb/c mice (Razi Institute, Karaj, Iran) weighing 20–25 g were housed under standard conditions in a controlled temperature (20 °C) and a light/dark cycle (12/12 h). Mice were individually anesthetized via intraperitoneal injection of ketamine (20 mg kg^{-1}) and xylazine (2 mg kg^{-1}) and an inhaled mixture of 20% (v/v) isoflurane and propylene glycol. The hair was removed around the surgical site and sterilized by 10% povidone–iodine. A suitable pocket for implant was created after incision at the dorsal skin. PES, SPES, and Ca-SPES scaffolds were implanted into 12 mice (n = 4 for each scaffold), and then the incision was closed with sutures.

Histopathology. A total of 12 weeks after implantation, mice were anesthetized and the implants were removed with surrounded tissue and were fixed in a 10% buffered formaldehyde solution, processed, and embedded in paraffin. Thick sections (3–5 μm) were prepared and stained with H&E, Masson's trichrome, and von Kossa. Finally, the stained sections were observed using a light microscope.

Statistical Analysis. All experiments were conducted at least three times. Data are expressed as mean ± standard deviation (SD). One-way analysis of variance (ANOVA) was used to compare the results. The P value for statistical significance is defined as $p < 0.05$. All statistical analysis was performed using *SPSS 11.0* software.

RESULTS

Scaffold Characterization. PES was sulfonated according to our previous report.[36] In the current research, high dimensional stability and suitable calcium-ion adsorption were provided by setting the degree of sulfonation to about 15 mol %. The physical characteristics of the fabricated scaffolds and polymer solutions are shown in Table 2. The viscosities of the SPES and PES solutions (at 30 °C) were measured as 2163 and 2267 cP, respectively. In addition, the conductivities of the solutions were determined to be 3.38 and 156.72 μs cm^{-1} for PES and SPES solutions, respectively. The proton conductivity of the SPES film was also demonstrated to be much higher than that of PES.

To investigate the sulfonation of PES, FTIR was performed on the prepared samples (Figure 1). In addition to the characteristic peaks of the PES spectrum, two new peaks were observed in the SPES spectrum near 970 and 1050 cm^{-1}, which are related to SO_3H stretching vibrations.[40] Another known characteristic peak of the SO_3H group near 1180 cm^{-1}, indicative of its asymmetrical vibrations, was not observed in SPES spectra because of overlapping.

Figures 2 and 3 show the SEM micrographs of the fabricated scaffolds. All scaffolds had a bead-free nanofibrous structure with interconnected pores. Image analysis of nanofibers

Table 2. Characterization of Scaffolds

polymer	solution viscosity (cP)	solution conductivity (μS)	scaffold porosity (%)	average fiber diameter (nm)	specific surface area (m^2 g^{-1})	proton conductivity (film, S cm^{-1})
PES	2163	3.38	74.32 ± 3.24	573 ± 145	4.84	0.000092
SPES	2267	156.72	77.64 ± 4.56	204 ± 63	12.13	0.00056
Ca-SPES			75.47 ± 4.68	212 ± 75	12.06	

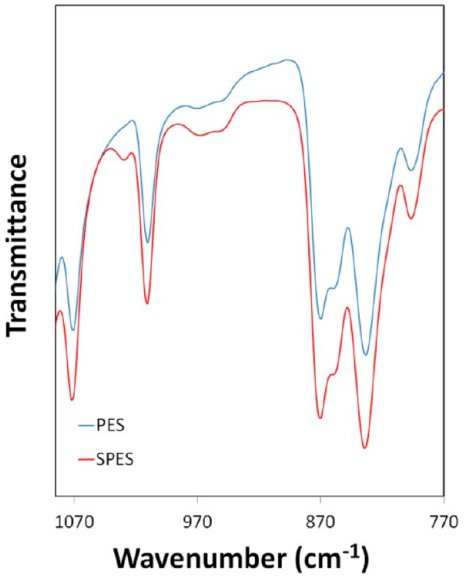

Figure 1. Attenuated total reflectance FTIR spectra of PES and SPES.

demonstrated a mean diameter of 573 ± 145 nm for PES, 204 ± 63 nm for SPES, and 212 ± 75 nm for Ca-SPES nanofibers. As seen in Figure 2c,f, SPES nanofibers were demonstrated to have a considerable decrease in diameter and had narrower diameter distribution and, consequently, a larger specific surface area. The latter was demonstrated by BET analysis, which was equal to 4.84 and 12.13 m^2 g^{-1} for PES and SPES nanofibers, respectively. No significant difference was observed between the porosities of the PES and SPES scaffolds. Also, according to Table 2, the physical properties of the Ca-SPES and SPES scaffolds were similar and there was no significant difference between their fiber sizes, porosities, and specific surface areas.

The SEM micrographs of SPES nanofibers after calcium ion exchange are depicted in Figure 3a,b. Qualitatively, no change was observed in the surface morphology of nanofibers compared to that observed before treatment. After ion exchange, EDX mapping was performed in order to detect calcium ions electrostatically attached to the SPES polymer chains (Figure 3c). Calcium ions were demonstrated as red dots distributed throughout the SPES nanofibers. To investigate the bioactivity, all scaffolds were immersed in SBF. After 7 days, the formation of the apatite layer was observed only on Ca-SPES nanofibers (Figure 3d,e), and no sign of apatite formation was detected on PES and SPES. EDX mapping also showed the existence of calcium and phosphorous atoms, as depicted in the micrograph, as red and green dots, respectively (Figure 3f).

In Vitro. To evaluate the potential of fabricated membranes as tissue-engineered scaffolds, stem cells were cultured on the surface of nanofibers and their proliferation, infiltration, and osteogenic differentiation were investigated in vitro. According to the MTT results (Figure 4), an increase in the cell population was detected during the period of study, even though no significant difference was observed between cell proliferations on different groups until day 2 of the experiment.

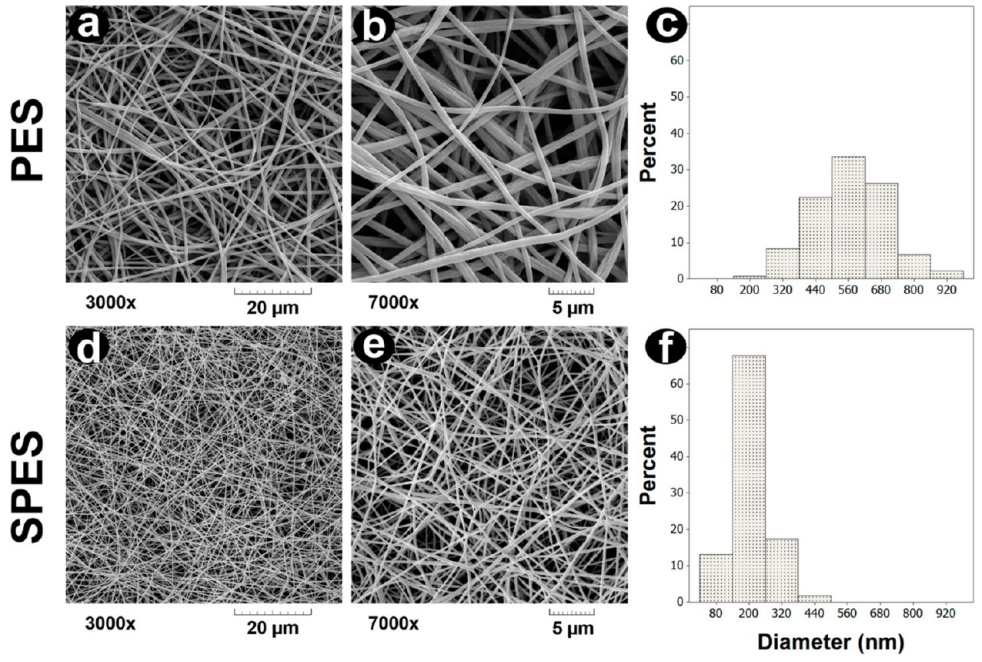

Figure 2. SEM micrographs of PES (a and b) and SPES (d and e) electrospun nanofibers at 3000× (a and d) and 7000× (b and e) magnification and histograms of the fiber diameter distributions for PES (c) and SPES (f) nanofibers.

dx.doi.org/10.1021/am404500c | ACS Appl. Mater. Interfaces 2014, 6, 72−82

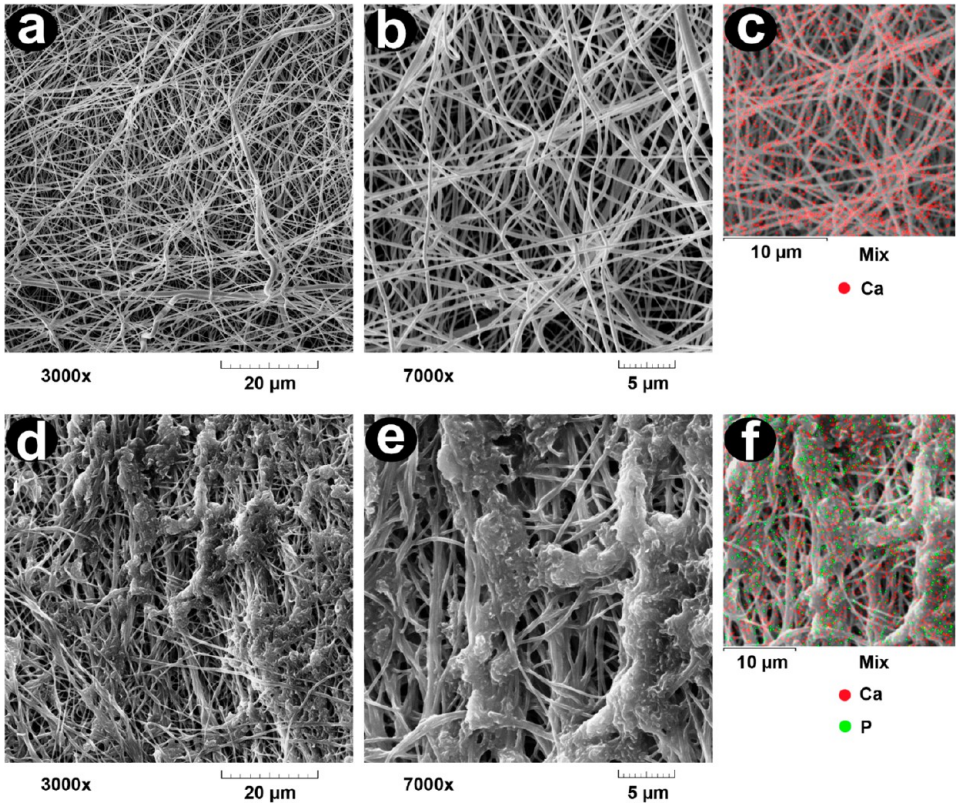

Figure 3. SEM micrographs of Ca-SPES (a and b) and SBF-soaked Ca-SPES (d and e) nanofibers at 3000× (a and d) and 7000× (b and e) magnification and EDX mapping of Ca-SPES (c) and SBF-soaked Ca-SPES (f) nanofibers. Calcium and phosphorous atoms are depicted as red and green dots, respectively.

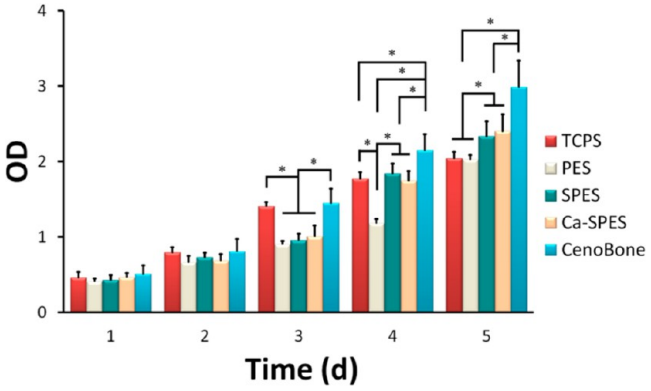

Figure 4. MTT cell proliferation assay of MSC on scaffolds, CenoBone, and TCPS during a 5-day culture period. Data are expressed as mean ± SD. Asterisks show significant differences with $p < 0.05$.

throughout the scaffolds after the period of culture under a growth medium (Figure 5).

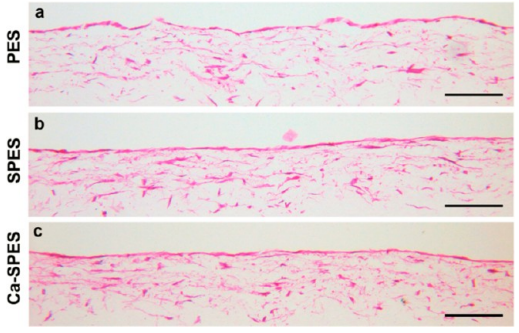

Figure 5. H&E-stained cross sections of cell-seeded PES (a), SPES (b), and Ca-SPES (c) nanofibrous scaffolds after 14 days of culture. Scale bars represent 250 μm.

In addition, a higher proliferation rate was observed on TCPS and CenoBone on day 3. Then, the proliferation rates increased on SPES, Ca-SPES, and CenoBone, and there was no significant difference between cell numbers on Ca-SPES and SPES on days 4 and 5. A higher cell population was observed on SPES and Ca-SPES compared with PES and TCPS on day 5. In addition, the greatest population of stem cells was observed on CenoBone compared with other groups.

According to the cross sections of cell-seeded scaffolds, it was found that stem cells infiltrated the inner layers of the nanofibers. A homogeneous distribution of cells was observed

In the present work, bone-specific gene expression, ALP activity, and calcium deposition were determined to investigate the osteogenic differentiation of stem cells cultured on various electrospun scaffolds. On the basis of real-time RT-PCR measurements (Figure 6), there was higher expression of the runx2 gene on all of the scaffold types in comparison with TCPS on day 7 of differentiation. On day 14, both SPES and Ca-SPES had significantly higher runx2 expression than PES and TCPS. Moreover, osteocalcin expression was detected to be higher on SPES and Ca-SPES in comparison to PES and TCPS on day 7. On day 14, osteocalcin expression of Ca-SPES

dx.doi.org/10.1021/am404500c | ACS Appl. Mater. Interfaces 2014, 6, 72−82

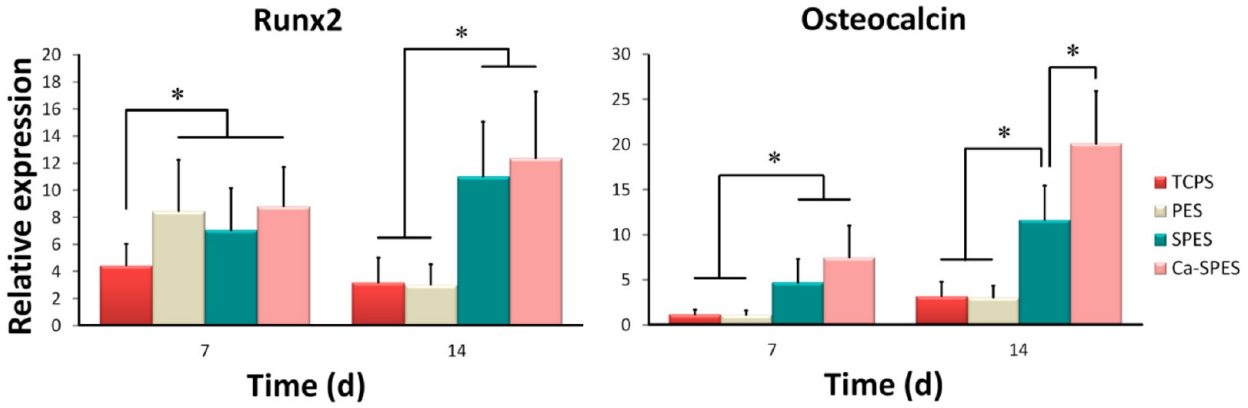

Figure 6. Relative expression of runx2 and osteocalcin on days 7 and 14 in MSC on scaffolds and TCPS during osteogenic differentiation. Data are expressed as mean ± SD. Asterisks show significant differences with $p < 0.05$.

increased higher than that on SPES, and its mRNA level reached a value greater than that of other scaffolds and TCPS.

Mineralization of stem cells on scaffolds and TCPS was first visualized using Alizarin Red staining on day 7 (Figure 7).

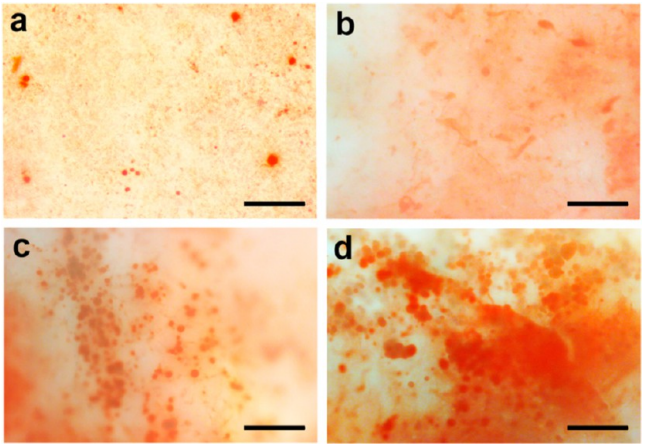

Figure 7. Alizarin Red staining of MSC on TCPS (a), PES (b), SPES (c), and Ca-SPES (d) nanofibers after a 7-day culture under an osteogenic medium. Scale bars represent 250 μm.

Because of the large amount of mineralization on day 14, different scaffolds were qualitatively similar after Alizarin Red staining (data not shown), so calcium content assay was performed to quantify mineral depositions. According to the findings (Figures 8 and 9), an increasing trend of ALP activity and calcium mineralization was observed during the period of study. Moreover, a higher amount of ALP activity was observed in cells on Ca-SPES and CenoBone compared to other scaffolds on days 7 and 14 of differentiation. In these time points, there was no significant difference between the enzyme activities of stem cells cultured on TCPS, PES, and SPES. The same pattern was observed from calcium content measurements. In both time points, the greatest calcium precipitation was determined on Ca-SPES scaffolds and CenoBone. On day 7, the calcium content was higher on SPES compared to PES and TCPS. There was also no significant difference between mineralization on SPES, PES, and TCPS after 14 days of differentiation. The process of differentiation was investigated through SEM images of differentiating stem cells on Ca-SPES on days 7 (Figure 10a,b) and 14 (Figure 10d,e). Mineral depositions were clearly obvious in both time points but with higher amounts and larger

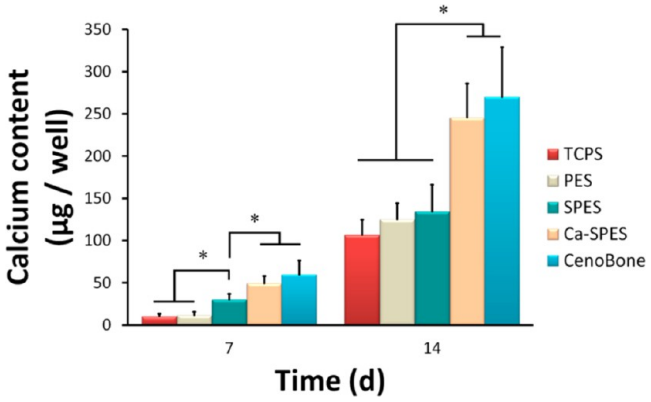

Figure 8. Calcium content of MSC on scaffolds, CenoBone, and TCPS during osteogenic differentiation. Data are expressed as mean ± SD. Asterisks show significant differences with $p < 0.05$.

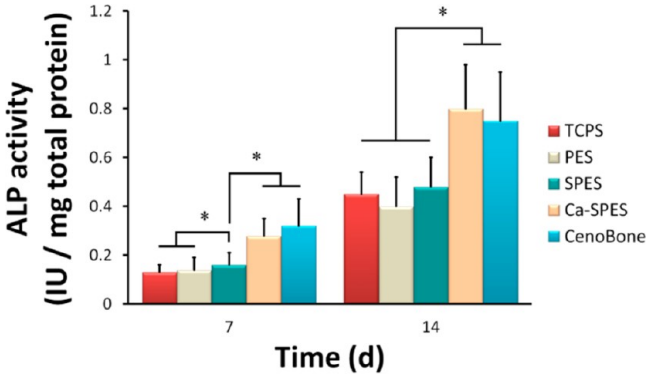

Figure 9. ALP activity of MSC on scaffolds, CenoBone, and TCPS during osteogenic differentiation. Data are expressed as mean ± SD. Asterisks show significant differences with $p < 0.05$.

aggregations on day 14. They also had a vividly porous structure composed from the aggregation of globular mineral accretions. EDX mapping also showed the existence of calcium and phosphorous atoms, as depicted in Figure 10c,f.

In Vivo. All of the animals survived until the scheduled time of sacrifice, and there were no general or local complications. A total of 12 weeks postimplantation, the skin of the mice was cut to retrieve the samples. In the macroscopic examination (Figure 11a–c), a significant difference was observed between the appearance and shapes of the scaffolds. In contrast to the PES

dx.doi.org/10.1021/am404500c | ACS Appl. Mater. Interfaces 2014, 6, 72–82

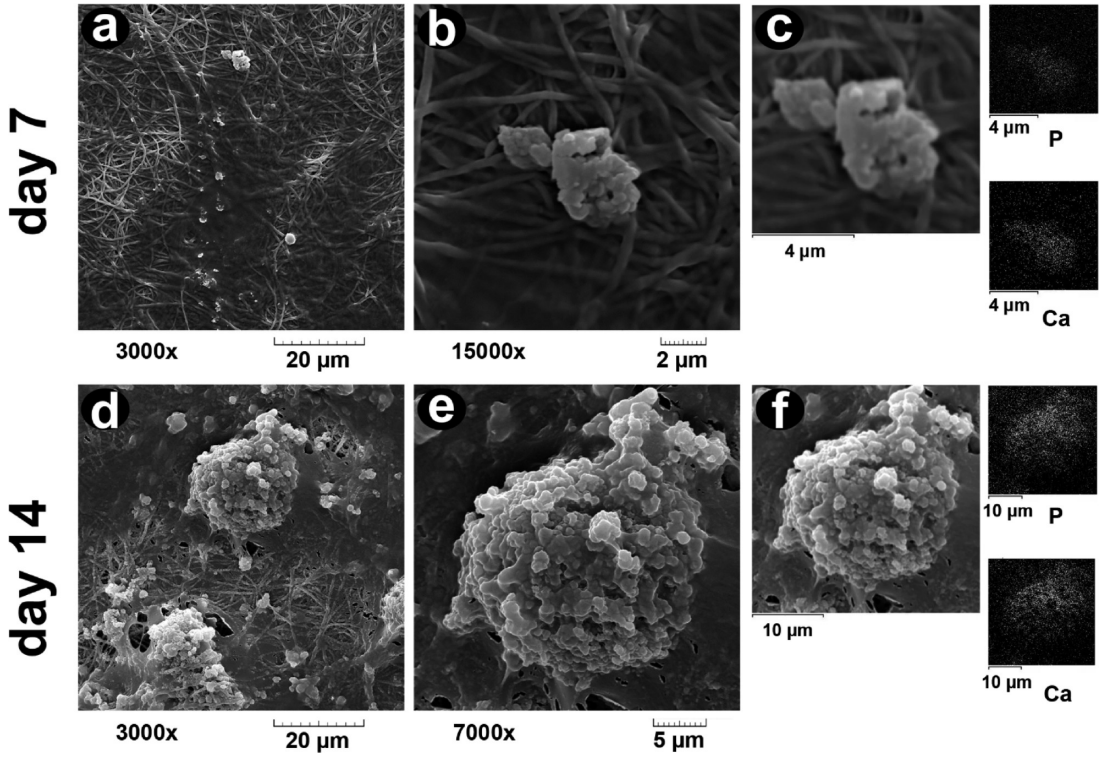

Figure 10. SEM micrographs of MSC during osteogenic differentiation on Ca-SPES nanofibers on days 7 (a and b) and 14 (d and e) and EDX mapping of mineral depositions on days 7 (c) and 14 (f).

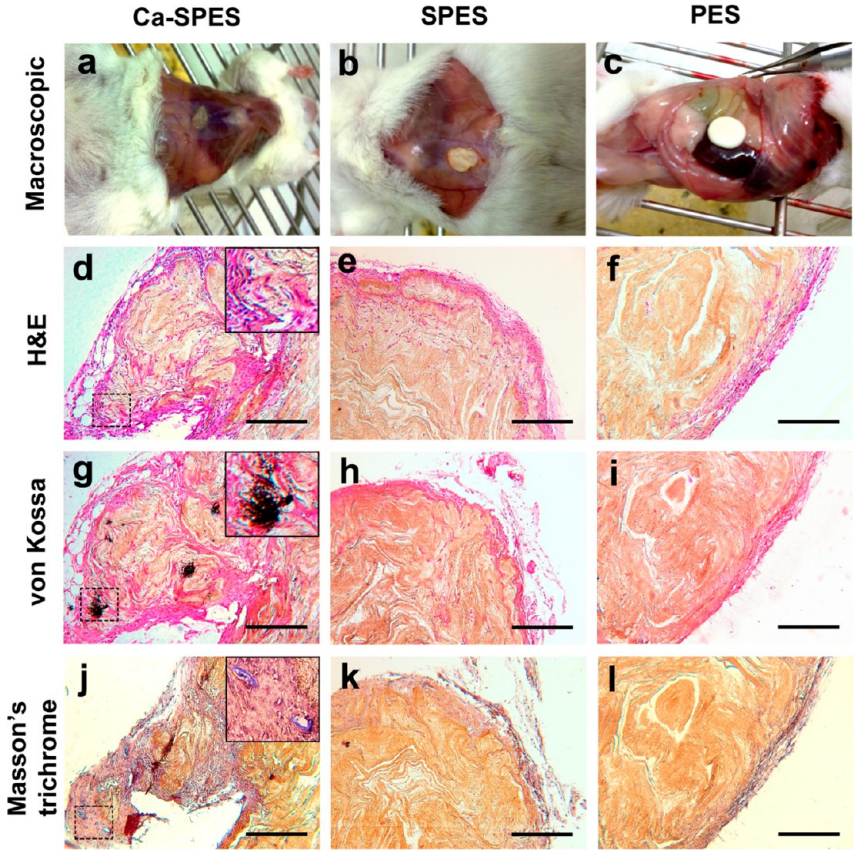

Figure 11. Macroscopic (a–c) and histological findings of ectopic bone formation, H&E staining (d–f), von Kossa staining (g–i), and Masson's trichrome (j–l) of Ca-SPES (a, d, g, and j), SPES (b, e, h, and k), and PES (c, f, i, and l). Scale bars represent 500 μm.

dx.doi.org/10.1021/am404500c | *ACS Appl. Mater. Interfaces* 2014, 6, 72–82

scaffold, which remained unchanged during implantation, SPES and Ca-SPES scaffolds showed a wrinkled structure and more interaction with the surrounding subcutaneous tissue. In addition, shrinkage and integration into the surrounding tissue were higher in Ca-SPES scaffolds in comparison with that observed in SPES.

Microscopic examination of the samples after H&E (Figure 11d–f), Masson's trichrome (Figure 11g–i), and von Kossa (Figure 11j–l) staining was performed under a light microscope. On all of the retrieved scaffold grafts, infiltration of the host cells and surrounding tissue was observable. In addition, H&E staining demonstrated that much more cells and surrounding tissue infiltrated into the Ca-SPES scaffolds in comparison to the others. Cellular distribution and infiltration were also higher in SPES scaffolds compared with PES. According to von Kossa staining, ectopic bone formation was only detected in Ca-SPES scaffolds and no evidence of mineralization was observed in SPES scaffolds or PES. In addition, Masson's trichrome staining was only positive in the samples of retrieved Ca-SPES scaffolds. The collagen fibers, stained in blue (Figure 11g), were similarly located in the mineralized areas of the same section (Figure 11j).

DISCUSSION

Because of the growing need for bone grafts, scientists have searched for new biomaterials and fabrication processes to synthesize tissue-engineered scaffolds. Mimicking the fibrous structure of ECM is an efficient strategy to design and fabricate scaffolds from appropriate biomaterials.[41] Recently, our research group introduced PES as a new substrate for the fabrication of BGSs.[12] We demonstrated that collagen grafting on electrospun PES membranes could efficiently enhance the infiltration and osteogenic differentiation of unrestricted somatic stem cells in vitro. Herein, we hypothesized that the existence of calcium ions in the structure of PES nanofibers would improve the bone tissue engineering properties of PES scaffolds. This idea came from the well-established effects of calcium ions on osteogenesis in various studies.[31−33,42] Calcium ion is one of the components of hydroxyapatite crystals, which form more than 70% of bone structure.[30] Indeed, enhanced osteogenic differentiation of cultured stem cells on hydroxyapatite structures has been linked to the calcium ions in its composition. Furthermore, this phenomenon is suggested to be responsible for enhanced regeneration of bone defects in implanted hydroxyapatite structures.[43,44] To put calcium ions on the polymer chains, PES was sulfonated to exhibit cation-exchange properties and calcium ions were subsequently exchanged with protons.

The porous and nanofibrous structure of electrospun scaffolds greatly mimics the topography of ECM and is ideal for bone tissue engineering applications. The viscosity of the SPES solution was slightly higher than that of PES, which may be due to better intermolecular interactions and, consequently, higher resistance to the movement of polymer chains caused by the addition of SO_3H groups.[45] In addition, PES showed a drastic increase in the solution conductivity after sulfonation, which was almost 50 times higher than that of neat PES. This could be due to the addition of anionic groups to the polymer chains after sulfonation. It is now widely known that an increase in the solution conductivity results in smaller fiber diameters and an increase in the solution viscosity leads to larger fiber diameters.[46] Herein, because of the negligible viscosity increase after sulfonation, the decrease of the fiber diameter is mostly influenced by the increased solution conductivity. The larger specific surface area of SPES nanofibers can be explained by the considerable decrease of their diameter. This is essential for tissue engineering applications because a higher specific surface area leads to a more efficient interaction between cells and the scaffold.[15]

The existence of sulfonic acid groups after the process of sulfonation was confirmed through FTIR spectroscopy. The characteristic peaks of the sulfonic acid group were detected at SPES spectra as previously reported.[40] Besides these peaks, absorbance at 1180 cm^{-1} is also linked to the asymmetrical vibrations in the sulfonic acid group. However, because of overlapping with the main peaks of PES, it was not observed in the FTIR spectrum after sulfonation.

Ca^{2+} ions are of great importance in some critical cell and tissue functions such as signaling, adhesion, proliferation, differentiation, and development.[47−49] The effect of calcium ions on the maturation of osteoblasts and in bone repair and regeneration has been well-documented.[50−52] To take advantage of this, we hypothesized that the incorporation of calcium ions in the structure of nanofibers would produce a bioactive surface suitable for bone regeneration applications. We accomplished this task via sulfonation and subsequent immersion in a calcium-ion-containing solution, and the ion-exchange reaction was confirmed via EDX mapping. It is worth noting that no sign of calcium ions was detected on PES scaffolds after immersion. It is indicative that sulfonic acid groups created in the structure of SPES nanofibers could capture calcium ions from the solution. This ion-exchange ability of SPES is in accordance with proton conductivity measurements. Interestingly, it was also shown that only Ca-SPES was able to induce the formation of the apatite layer on the surface of nanofibers in a 7-day period. These data demonstrate the bioactivity of Ca-SPES scaffolds and their high potential for use in bone tissue engineering applications. The incorporation of negatively charged groups to functionalize polymeric materials has been previously reported. The Kamitakahara group has functionalized the polyamides with carboxyl[53] and sulfonic acid groups[54] and showed apatite formation on polymeric films after the incorporation of calcium ions and further immersion in SBF. In another study, Leonor et al.[34] sulfonated different polymers and investigated the formation of the apatite layer after $Ca(OH)_2$ treatment and immersion in SBF. They detected formation of the apatite layer only after treatment of the surface-functionalized polymers with a solution containing calcium ions, which is also in accordance with our results. However, none of the mentioned researches have evaluated the capability of the polymers for bone regeneration and osteogenesis, neither in vitro nor in vivo.

Stem cells benefit from two important characteristics: self-renewal and multilineage differentiation potential. These properties make them ideal for cell therapy and tissue engineering applications.[55] Recently, stem cells, in combination with biomaterials, have attracted lots of interest in the field of tissue engineering.[56,57] Herein, we evaluated the potential of fabricated scaffolds to support the proliferation and osteogenic differentiation of MSC in vitro. All nanofibrous scaffolds were shown to be noncytotoxic and able to support the proliferation of stem cells compared to that observed on TCPS and CenoBone. In addition, a higher rate of cell proliferation was observed on nanofibrous scaffolds in comparison with TCPS after day 4. This may be due to the fact that LEAE is capable of producing 3D structures. On the basis of H&E staining of the

cross sections, stem cells were demonstrated to infiltrate the 3D electrospun scaffolds after growing to confluency on the surface, a process that did not happen on TCPS and led to a decreased rate of proliferation on the late days. The higher cell population on SPES and Ca-SPES may be due to the existence of anionic groups, which contributed to a higher rate of cell proliferation, as shown by other researchers.[58,59] The high rate of cell proliferation on CenoBone can be explained by the fact that this BGS exhibits a 3D structure composed of biological materials that are highly attractive for cells to attach to and proliferate.

Osteogenesis of stem cells was also investigated on different scaffolds, CenoBone, and TCPS. ALP is a critical enzyme in the process of differentiation of stem cells toward osteoblastic lineage and is responsible for cleaving phosphate groups and initiating biomineralization.[60] Both ALP activity and calcium deposition were demonstrated to be higher on Ca-SPES scaffolds compared with other scaffolds and TCPS. Because there was no significant difference between the physical properties of Ca-SPES and SPES scaffolds, the observed results were only due to their different chemical properties. These data indicate the effect of calcium ions as signaling ligands, enhancing osteogenic differentiation of stem cells. The higher amount of biomineralization on SPES may be due to the effect of sulfonic acid groups in the initial nucleation step for mineralization.[61] CenoBone is a commercial BGS that is currently used to treat bone defects, and its healing effect is comparable with autogenous bone grafting.[62] Interestingly, fabricated Ca-SPES scaffolds could enhance osteogenic differentiation of stem cells as much as CenoBone did. In contrast to Ca-SPES, which is based on a synthetic polymeric material, CenoBone is actually a partially demineralized freeze-dried bone matrix. These two scaffolds also differ in their physical structure because Ca-SPES is composed of electrospun nanofibers while Cenobone exhibits a foamlike freeze-dried structure. On the other hand, both Ca-SPES and commercial CenoBone exhibit a 3D and highly porous structure, which is so appropriate for guided bone regeneration. In addition, calcium ions are present in the structure of both Ca-SPES and Cenobone and enable them to contribute to the process of osteogenesis. For a closer look at the osteogenic behavior of MSC, expression of bone-related genes was also monitored. Runx2 is a major gene responsible for the early orientation of stem cells toward osteoblastic lineage.[63] The data on day 7 of the study demonstrated that the nanofibrous structure of scaffolds contributed to the higher expression of this gene compared to that on TCPS. This was according to the reports on the capacity of nanofibers for the enhancement of stem cell differentiation.[64,65] Osteocalcin has an important role in biomineralization and is expressed in the late stages of osteogenesis.[66] Interestingly, this gene showed a higher expression on Ca-SPES compared to other scaffolds on day 14. This can be due to the role of calcium in the upregulation of osteogenic genes and can explain the higher mineral deposition on this scaffold. In our previous study, we developed a new scaffold composed of poly(L-lactide) nanofibers coated with nanohydroxyapatite. There, we demonstrated its osteoinductivity and formation of ectopic bone after subcutaneous implantation. Interestingly, in the present study, the Ca-SPES scaffold was also demonstrated to be osteoinductive. Indeed, no sign of bone formation was observed after the implantation of other scaffolds. Mineralization in the samples of Ca-SPES is suggested to be ectopic bone formation because of detection of collagen production in the mineralized areas. Osteoinduction of biomaterials has been shown in some previous studies.[22,67−69] Herein, the incorporation of calcium ions in nanofibrous scaffolds was shown to guide bone formation during subcutaneous implantation. This is explained by the fact that Ca-SPES is able to induce the formation of an apatite layer in vivo in accordance with the results from immersion of the scaffolds in SBF in vitro. Some days postimplantation, the apatite aggregates would form and subsequently contribute to mineralization and ectopic bone formation in the surrounding tissue as reported previously.[70]

It is worth stating that not every ion-exchange polymer can be processed into electrospun nanofibers in order to fabricate calcium-ion-incorporated scaffolds. In addition, the range of the fiber diameter is limited based on the type of polymer and technical conditions. The incorporation of calcium ions into scaffolds gives rise to a new alternative approach to the current strategy, which combines the polymers and bioceramics. Polymeric materials exhibit a high ability to be processed into various shapes and structures.[71] In this approach, scaffolds with appropriate physical and chemical characteristics can be fabricated from desired polymers. In the next step, the incorporation of calcium ions via simple modifications will make the scaffolds bioactive and ideal for bone tissue engineering applications. So, we believe that the Ca-SPES scaffold is an improvement of the currently used BGS because of not only its similar osteogenic capacity but also the easiness and cost-effectiveness of the fabrication process. For further improvements, suitable inducers and growth factors can be added to Ca-SPES in order to optimize the host tissue response.

Here, we report for the first time that the incorporation of calcium ions in scaffolds gives them the capability enhancing the osteogenic differentiation of stem cells and inducing bone formation in ectopic sites. This ability is very significant for a BGS to be used in bone regeneration applications.

■ CONCLUSION

In the present study, ion-exchange nanofibrous membranes were fabricated via electrospinning of SPES. We demonstrated that the incorporation of calcium ions into SPES nanofibrous scaffolds gave them the ability to enhance osteogenic differentiation of stem cells in vitro. These enhancements were confirmed at the level of gene expression, biomineralization, and enzyme activity analyses. In addition, the Ca-SPES electrospun scaffold showed the capacity for ectopic bone formation in the absence of exogenous cells. These scaffolds hold promising potential for application as BGS in the treatment of bone damage.

■ AUTHOR INFORMATION

Corresponding Author

*E-mail: haddadi@aut.ac.ir.

Notes

The authors declare no competing financial interest.

■ ACKNOWLEDGMENTS

We acknowledge funding for this study provided by the Stem Cell Technology Research Center (Tehran, Iran). The authors thank Mahmoud Naderi, Reza Ardeshiri-lajimi, Majid Mosahebi, and Abbas Shafiee for technical assistance.

REFERENCES

(1) Giannoudis, P. V.; Dinopoulos, H.; Tsiridis, E. *Injury* **2005**, *36*, S20−27.
(2) Salgado, A. J.; Coutinho, O. P.; Reis, R. L. *Macromol. Biosci.* **2004**, *4*, 743−765.
(3) Damien, C. J.; Parsons, J. R. *J. Appl. Biomater.* **1991**, *2*, 187−208.
(4) Moore, W. R.; Graves, S. E.; Bain, G. I. *ANZ J. Surg.* **2001**, *71*, 354−361.
(5) Kujala, S.; Ryhanen, J.; Danilov, A.; Tuukkanen, J. *Biomaterials* **2003**, *24*, 4691−4697.
(6) Bucholz, R. W. *Clin. Orthop. Relat. Res.* **2002**, 44−52.
(7) Cook, S. D.; Dalton, J. E.; Prewett, A. B.; Whitecloud, T. S. *Spine* **1995**, *20*, 877−886.
(8) Hosseinkhani, H.; Hosseinkhani, M.; Khademhosseini, A.; Kobayashi, H. *J. Controlled Release* **2007**, *117*, 380−386.
(9) Lewandrowski, K. U.; Bondre, S. P.; Wise, D. L.; Trantolo, D. J. *Biomed. Mater. Eng.* **2003**, *13*, 115−124.
(10) Miki, T.; Masaka, K.; Imai, Y.; Enomoto, S. *J. Craniomaxillofac. Surg.* **2000**, *28*, 294−299.
(11) Kim, C. W.; Talac, R.; Lu, L.; Moore, M. J.; Currier, B. L.; Yaszemski, M. J. *J. Biomed. Mater. Res., Part A* **2008**, *85*, 1114−1119.
(12) Shabani, I.; Haddadi-Asl, V.; Soleimani, M.; Seyedjafari, E.; Babaeijandaghi, F.; Ahmadbeigi, N. *Tissue Eng., Part A* **2011**, *17*, 1209−1218.
(13) Barzin, J.; Feng, C.; Khulbe, K.; Matsuura, T.; Madaeni, S.; Mirzadeh, H. *J. Membr. Sci.* **2004**, *237*, 77−85.
(14) Pless, G. *Methods Mol. Biol.* **2010**, *640*, 511−523.
(15) Jang, J. H.; Castano, O.; Kim, H. W. *Adv. Drug Delivery Rev.* **2009**, *61*, 1065−1083.
(16) Ramakrishna, S.; Fujihara, K.; Teo, W. E.; Yong, T.; Ma, Z.; Ramaseshan, R. *Mater. Today* **2006**, *9*, 40−50.
(17) Li, C.; Vepari, C.; Jin, H. J.; Kim, H. J.; Kaplan, D. L. *Biomaterials* **2006**, *27*, 3115−3124.
(18) Seyedjafari, E.; Soleimani, M.; Ghaemi, N.; Shabani, I. *Biomacromolecules* **2010**.
(19) Shin, H. J.; Lee, C. H.; Cho, I. H.; Kim, Y. J.; Lee, Y. J.; Kim, I. A.; Park, K. D.; Yui, N.; Shin, J. W. *J. Biomater. Sci., Polym. Ed.* **2006**, *17*, 103−119.
(20) Thorvaldsson, A.; Stenhamre, H.; Gatenholm, P.; Walkenstrom, P. *Biomacromolecules* **2008**, *9*, 1044−1049.
(21) Zhou, Y.; Yang, D.; Chen, X.; Xu, Q.; Lu, F.; Nie, J. *Biomacromolecules* **2008**, *9*, 349−354.
(22) Babaeijandaghi, F.; Shabani, I.; Seyedjafari, E.; Naraghi, Z. S.; Vasei, M.; Haddadi-Asl, V.; Hesari, K. K.; Soleimani, M. *Tissue Eng., Part A* **2010**, *16*, 3527−3536.
(23) Riboldi, S. A.; Sampaolesi, M.; Neuenschwander, P.; Cossu, G.; Mantero, S. *Biomaterials* **2005**, *26*, 4606−4615.
(24) Pham, Q. P.; Sharma, U.; Mikos, A. G. *Biomacromolecules* **2006**, *7*, 2796−2805.
(25) Baker, B. M.; Gee, A. O.; Metter, R. B.; Nathan, A. S.; Marklein, R. A.; Burdick, J. A.; Mauck, R. L. *Biomaterials* **2008**, *29*, 2348−2358.
(26) Nam, J.; Huang, Y.; Agarwal, S.; Lannutti, J. *Tissue Eng.* **2007**, *13*, 2249−2257.
(27) Zhu, X.; Cui, W.; Li, X.; Jin, Y. *Biomacromolecules* **2008**, *9*, 1795−1801.
(28) Shabani, I.; Haddadi-Asl, V.; Seyedjafari, E.; Soleimani, M. *Biochem. Biophys. Res. Commun.* **2012**, *423*, 50−54.
(29) Pilliar, R. M.; Filiaggi, M. J.; Wells, J. D.; Grynpas, M. D.; Kandel, R. A. *Biomaterials* **2001**, *22*, 963−972.
(30) Laurencin, C.; Khan, Y.; El-Amin, S. F. *Expert Rev. Med. Devices* **2006**, *3*, 49−57.
(31) Maeno, S.; Niki, Y.; Matsumoto, H.; Morioka, H.; Yatabe, T.; Funayama, A.; Toyama, Y.; Taguchi, T.; Tanaka, J. *Biomaterials* **2005**, *26*, 4847−4855.
(32) McCullen, S. D.; Zhan, J.; Onorato, M. L.; Bernacki, S. H.; Loboa, E. G. *Tissue Eng., Part A* **2010**, *16*, 1971−1981.
(33) Nakade, O.; Takahashi, K.; Takuma, T.; Aoki, T.; Kaku, T. *J. Bone Miner. Metab.* **2001**, *19*, 13−19.
(34) Leonor, I. B.; Kim, H. M.; Balas, F.; Kawashita, M.; Reis, R. L.; Kokubo, T.; Nakamura, T. *J. Mater. Sci.: Mater. Med.* **2007**, *18*, 1923−1930.
(35) Leonor, I. B.; Kim, H. M.; Balas, F.; Kawashita, M.; Reis, R. L.; Nakamura, T. *Key Eng. Mater.* **2005**, *284*, 453−456.
(36) Shabani, I.; Hasani-Sadrabadi, M. M.; Haddadi-Asl, V.; Soleimani, M. *J. Membr. Sci.* **2011**, *368*, 233−240.
(37) Kim, I.; Choi, J.; Tak, T. *J. Appl. Polym. Sci.* **1999**, *74*, 2046−2055.
(38) Leonor, I. B.; Balas, F.; Kawashita, M.; Reis, R. L.; Kokubo, T.; Nakamura, T. *J. Biomed. Mater. Res., Part B* **2009**, *91*, 239−247.
(39) Shayesteh, Y. S.; Khojasteh, A.; Soleimani, M.; Alikhasi, M.; Khoshzaban, A.; Ahmadbeigi, N. *Oral Surg., Oral Med., Oral Pathol., Oral Radiol. Endod.* **2008**, *106*, 203−209.
(40) Lu, D.; Zou, H.; Guan, R.; Dai, H.; Lu, L. *Polym. Bull.* **2005**, *54*, 21−28.
(41) Murugan, R.; Ramakrishna, S. *Tissue Eng.* **2007**, *13*, 1845−1866.
(42) Park, J. W.; Suh, J. Y.; Chung, H. J. *J. Biomed. Mater. Res., Part A* **2008**, *86*, 117−126.
(43) Muller, P.; Bulnheim, U.; Diener, A.; Luthen, F.; Teller, M.; Klinkenberg, E. D.; Neumann, H. G.; Nebe, B.; Liebold, A.; Steinhoff, G.; Rychly, J. *J. Cell. Mol. Med.* **2008**, *12*, 281−291.
(44) Yoshikawa, H.; Myoui, A. *J. Artif. Organs* **2005**, *8*, 131−136.
(45) Lufrano, F.; Squadrito, G.; Patti, A.; Passalacqua, E. *J. Appl. Polym. Sci.* **2000**, *77*, 1250−1256.
(46) Mit-uppatham, C.; Nithitanakul, M.; Supaphol, P. *Macromol. Chem. Phys.* **2004**, *205*, 2327−2338.
(47) Clapham, D. E. *Cell* **2007**, *131*, 1047−1058.
(48) Schroder, U. *J. Dent. Res.* **1985**, *64*, 541−548.
(49) Durham, A. C.; Walton, J. M. *Biosci. Rep.* **1982**, *2*, 15−30.
(50) Zayzafoon, M. *J. Cell. Biochem.* **2006**, *97*, 56−70.
(51) Hauschka, P. V.; Lian, J. B.; Gallop, P. M. *Proc. Natl. Acad. Sci. U.S.A.* **1975**, *72*, 3925−3929.
(52) Anderson, J. J. *J. Nutr.* **1996**, *126*, 1153S−1158S.
(53) Miyazaki, T.; Ohtsuki, C.; Akioka, Y.; Tanihara, M.; Nakao, J.; Sakaguchi, Y.; Konagaya, S. *J. Mater. Sci.: Mater. Med.* **2003**, *14*, 569−574.
(54) Kawai, T.; Ohtsuki, C.; Kamitakahara, M.; Miyazaki, T.; Tanihara, M.; Sakaguchi, Y.; Konagaya, S. *Biomaterials* **2004**, *25*, 4529−4534.
(55) Bianco, P.; Riminucci, M.; Gronthos, S.; Robey, P. G. *Stem Cells* **2001**, *19*, 180−192.
(56) Sundelacruz, S.; Kaplan, D. L. *Semin. Cell Dev. Biol.* **2009**, *20*, 646−655.
(57) Sterodimas, A.; de Faria, J.; Nicaretta, B.; Pitanguy, I. *J. Plast. Reconstr. Aesthet. Surg.* **2010**, *63*, 1886−1892.
(58) Luna, S. M.; Silva, S. S.; Gomes, M. E.; Mano, J. F.; Reis, R. L. *J. Biomater. Appl.* **2011**, *26*, 101−116.
(59) Yamaguchi, M.; Shinbo, T.; Kanamori, T.; Wang, P. C.; Niwa, M.; Kawakami, H.; Nagaoka, S.; Hirakawa, K.; Kamiya, M. *J. Artif. Organs* **2004**, *7*, 187−193.
(60) Anderson, H. C.; Sipe, J. B.; Hessle, L.; Dhanyamraju, R.; Atti, E.; Camacho, N. P.; Millan, J. L. *Am. J. Pathol.* **2004**, *164*, 841−847.
(61) Chen, J.; Chu, B.; Hsiao, B. S. *J. Biomed. Mater. Res., Part A* **2006**, *79*, 307−317.
(62) Abolfazli, N.; Saleh Saber, F.; Lafzi, A.; Eskandari, A.; Mehrasbi, S. *J. Dent. Res. Dent. Clin. Dent. Prospects* **2008**, *2*, 1−8.
(63) Viereck, V.; Siggelkow, H.; Tauber, S.; Raddatz, D.; Schutze, N.; Hufner, M. *J. Cell. Biochem.* **2002**, *86*, 348−356.
(64) Seyedjafari, E.; Soleimani, M.; Ghaemi, N.; Sarbolouki, M. N. *J. Mater. Sci.: Mater. Med.* **2011**, *22*, 165−174.
(65) Binulal, N. S.; Deepthy, M.; Selvamurugan, N.; Shalumon, K. T.; Suja, S.; Mony, U.; Jayakumar, R.; Nair, S. V. *Tissue Eng., Part A* **2010**, *16*, 393−404.
(66) Roach, H. I. *Cell Biol. Int.* **1994**, *18*, 617−628.
(67) Yamasaki, H.; Sakai, H. *Biomaterials* **1992**, *13*, 308−312.
(68) Ripamonti, U. *Biomaterials* **1996**, *17*, 31−35.
(69) Habibovic, P.; Yuan, H.; van der Valk, C. M.; Meijer, G.; van Blitterswijk, C. A.; de Groot, K. *Biomaterials* **2005**, *26*, 3565−3575.

(70) Fujibayashi, S.; Neo, M.; Kim, H. M.; Kokubo, T.; Nakamura, T. *Biomaterials* **2004**, *25*, 443−450.
(71) Liu, X.; Ma, P. X. *Ann. Biomed. Eng.* **2004**, *32*, 477−486.